

LHC Searches for Top-philic Kaluza-Klein Graviton

Chao-Qiang Geng^{1,2,3*}, Da Huang^{4†}, Kimiko Yamashita^{2,3‡}

¹*Chongqing University of Posts & Telecommunications, Chongqing, 400065, China*

²*Physics Division, National Center for Theoretical Sciences, Hsinchu, Taiwan 300*

³*Department of Physics, National Tsing Hua University, Hsinchu, Taiwan 300*

⁴*Institute of Theoretical Physics, Faculty of Physics, University of Warsaw, Pasteura 5, 02-093 Warsaw, Poland*

**geng@phys.nthu.edu.tw*, †*dahuang@fuw.edu.pl*, ‡*kimikoy@phys.nthu.edu.tw*

Abstract

We study the phenomenology of a massive graviton G with non-universal couplings to the Standard Model (SM) particles. Such a particle can arise as a warped Kaluza-Klein graviton from a framework of the Randall-Sundrum extra-dimension model. In particular, we consider a case in which G is top-philic, i.e., G interacts strongly with the right-handed top quark, resulting in the large top-loop contributions to its production via the gluon fusion and its decays to the SM gauge bosons. We take into account the constraints from the current 13 TeV LHC data on the channels of $t\bar{t}$, $\gamma\gamma$, $jj(gg)$, γZ , and ZZ . Consequently, it is found that the strongest limit for this spin-2 resonance G comes from the $t\bar{t}$ pair search, which constrains the cutoff scale to be of $\mathcal{O}(100 \text{ GeV})$ for the right-top coupling of $\mathcal{O}(1)$ and the massive graviton mass in the range $m_G = 2\text{--}5 \text{ TeV}$, significantly relaxed compared with the universal G coupling case.

1 Introduction

Randall-Sundrum (RS) model [1] has an attractive feature as providing an explanation of the gauge hierarchy, $\mathcal{O}(10^{16})$, between the reduced Planck mass and electroweak scales. Not only solving the puzzle, it also has a nice potential to connect dark matter [2, 3, 4, 5] as its prediction of the Kaluza-Klein (KK) graviton naturally interacts with all of particles via each energy-momentum tensor.

It is known that the RS model of the universal coupling case (i.e. the KK graviton interacts with particles with the same coupling strength) suffers from strong constraints on the model parameters from the current LHC experimental results [4]. It is necessary to reconsider the non-universal case of the RS model ([6, 7, 8, 9, 10, 11, 12, 13]) from the latest LHC experimental data and explore the corresponding constraints for the model. One of such a case is that the KK graviton interacts strongly with the top quark, in which it was found that top-loop effects can be comparable with the tree-level ones for the KK graviton productions and its decays [14]. For simplicity, we concentrate on that only the right-handed top quark interacts with the KK graviton via a coupling of $\mathcal{O}(1)$, whereas the profile of the left-handed top quark is far away (UV brane) from a KK graviton wave function, which is localized near the IR brane. We assume that the color $SU(3)_c$ and hypercharge $U(1)_Y$ gauge fields are in the bulk, so that the couplings with the KK gravitons are diluted by a volume factor. The other Standard Model (SM) particles are localized near the UV brane. For this setup, our signals are $t\bar{t}$, $\gamma\gamma$, $jj(gg)$, γZ , and ZZ . We will derive the constraints on the model parameters from the latest 13 TeV LHC searches for the KK graviton resonance decaying to these final states.

The article is organized as follows. Our model is presented in Sec. 2, and the effective couplings by top-loops are described in Sec. 3. The KK graviton productions and decays are shown in Sec. 4 and Sec. 5, respectively. Constraints on the model parameters by the current 13 TeV LHC are discussed in Sec. 6. The summary is given in Sec. 7.

2 Top-philic KK Graviton Model

Besides being a possible solution to the gauge hierarchy problem, the generalized RS models provide us with a general framework to study the massive KK graviton with non-universal couplings to the SM fields. In this framework, the geometry

is a slice of a five-dimensional (5D) warped spacetime with two boundaries corresponding to UV and IR branes, respectively. All of the SM fields are promoted to 5-dimensional objects, either propagating in the bulk or located on the branes. The interactions among particles are given by the overlapping wave-functions of the involving particles, which naturally give rise to the hierarchy in the model couplings. In particular, the wave-function of the first KK graviton G is peaked near the IR brane, so that the fields located on or around the IR brane would couple to this massive graviton strongly, while other fields near the UV brane would have exponentially smaller couplings with G . Concretely, we can write down the following general interactions between G and SM particles

$$\mathcal{L} = - \sum_i \frac{c_i}{\Lambda} G_{\mu\nu} T_i^{\mu\nu}, \quad (1)$$

where $T_i^{\mu\nu}$ denotes the energy-momentum tensor for the i -th SM particle with c_i the corresponding the coupling strength, and Λ is the typical cutoff scale for the G interactions. In the simple case when the 5D bulk geometry is the AdS_5 spacetime with its curvature k and its length L , the mass and cutoff scale of this KK graviton is predicted to be $m_G \approx 3.8ke^{-kL}$ and $\Lambda \sim \bar{M}_{\text{Pl}}e^{-kL}$, respectively, where \bar{M}_{Pl} is the reduced Planck mass in the ordinary 4-dimensional spacetime.

In the present work, we consider a model in which only the right-handed top quark field sits around the IR brane, and the gauge bosons G_μ and B_μ corresponding to the color $SU(3)_c$ and hypercharge $U(1)_Y$ gauge groups live in the bulk, while other SM fields, including the $SU(2)_L$ gauge and SM Higgs doublet bosons, are placed close to or exactly on the UV brane. According to the naive dimensional analysis, G is expected to interact with the right-handed top quark strongly, while weakly with W^\pm and SM Higgs bosons and other fermions. Furthermore, the wave-functions of the zero-mode gauge fields are always predicted to be constant in the bulk, so that their couplings to G would be suppressed by the volume factor of order $1/\ln(\bar{M}_{\text{Pl}}/M_{\text{IR}}) \sim 1/(kL) \sim 0.03$ with the IR brane scale at $\mathcal{O}(\text{TeV})$. Note that this suppression factor has the similar order as the one-loop ones of $\alpha_{(s)}/(4\pi)$ for the EW (color) gauge bosons, with $\alpha_{(s)}$ referring to the electromagnetic (strong) fine structure constant. In the light of this observation, the interacting Lagrangian relevant to the phenomenology of the KK graviton is given by

$$\mathcal{L}_G = -\frac{G_{\mu\nu}}{\Lambda} \left[\frac{\alpha c_1}{4\pi} \left(\frac{1}{4} \eta^{\mu\nu} B^{\lambda\rho} B_{\lambda\rho} - B^{\mu\lambda} B^\nu{}_\lambda \right) + \frac{\alpha_s c_{gg}}{4\pi} \left(\frac{1}{4} \eta^{\mu\nu} G^{a\lambda\rho} G_{\lambda\rho}^a - G^{a\mu\lambda} G^{a\nu}{}_\lambda \right) \right]$$

$$\begin{aligned}
& +c_{tt} \left(\frac{i}{4} \bar{t}_R (\gamma^\mu D^\nu + \gamma^\nu D^\mu) t_R - \frac{i}{4} (D^\mu \bar{t}_R \gamma^\nu + D^\nu \bar{t}_R \gamma^\mu) t_R \right. \\
& \left. - i\eta^{\mu\nu} [\bar{t}_R \gamma^\rho D_\rho t_R - \frac{1}{2} D^\rho (\bar{t}_R \gamma_\rho t_R)] \right) \Big], \tag{2}
\end{aligned}$$

where $\eta_{\mu\nu} = \text{diag}(1, -1, -1, -1)$ is the Minkowski metric tensor, and $D_\mu = \partial_\mu + i(2/3)g_1 B_\mu + ig_s G_\mu^a$ is the covariant derivative for the right-handed top quark field. Note that in Eq. (2) we have explicitly picked up one-loop gauge factors in front of the corresponding massive graviton couplings to SM gauge bosons, in order to explicitly represent the aforementioned bulk volume suppression factors. With this convention, the couplings c_1 and c_{gg} are of $\mathcal{O}(1)$, resulting in the coupling sizes of

$$c_{tt} > \frac{\alpha_s c_{gg}}{4\pi} \sim \frac{\alpha c_1}{4\pi} \gg c_{\text{others}}. \tag{3}$$

After the spontaneous EW symmetry breaking, the original coupling between G and the $U(1)_Y$ gauge field B_μ is divided to the couplings with the electromagnetic A_μ and weak Z_μ fields as follows

$$\begin{aligned}
\mathcal{L}_G \supset & -\frac{1}{\Lambda} G_{\mu\nu} \left[\frac{\alpha c_{\gamma\gamma}}{4\pi} \left(\frac{1}{4} \eta^{\mu\nu} A^{\lambda\rho} A_{\lambda\rho} - A^{\mu\lambda} A^\nu{}_\lambda \right) + \frac{\alpha c_{Z\gamma}}{4\pi} \left(\frac{1}{4} \eta^{\mu\nu} A^{\lambda\rho} Z_{\lambda\rho} - A^{\mu\lambda} Z^\nu{}_\lambda \right) \right. \\
& \left. + \frac{\alpha c_{ZZ}}{4\pi} \left(\frac{1}{4} \eta^{\mu\nu} Z^{\lambda\rho} Z_{\lambda\rho} - Z^{\mu\lambda} Z^\nu{}_\lambda \right) \right], \tag{4}
\end{aligned}$$

where the couplings of $c_{\gamma\gamma, Z\gamma, ZZ}$ can be derived from that of c_1 with the transformations

$$\begin{aligned}
c_{\gamma\gamma} &= c_1 \cos^2 \theta_W, \quad c_{Z\gamma} = -c_1 \sin 2\theta_W = -\sin 2\theta_W c_{\gamma\gamma} / \cos^2 \theta_W, \\
c_{ZZ} &= c_1 \sin^2 \theta_W = \tan^2 \theta_W c_{\gamma\gamma}, \tag{5}
\end{aligned}$$

which is a particular case studied in Ref. [15]. As a result, there are only three free parameters c_{gg} , c_{tt} and c_1 to characterize the LHC signals of the KK graviton.

Since the SM Higgs boson is placed far away from the IR brane, the model cannot solve the hierarchy problem with the large warped factor in the original RS proposals. Also we would like to point out that with the completely UV localized left-handed and IR localized right-handed top quarks, it is difficult to generate the top quark mass [16, 17]. In fact, we do not require left-handed and right-handed top fields are strictly placed on the UV and IR branes, respectively, so that the overlap of these two fields in the bulk can generate top mass term, even though a large amount of tuning of 5D parameters is needed to achieve its observed large value. However, our focus here is the LHC phenomenology for the top-philic KK

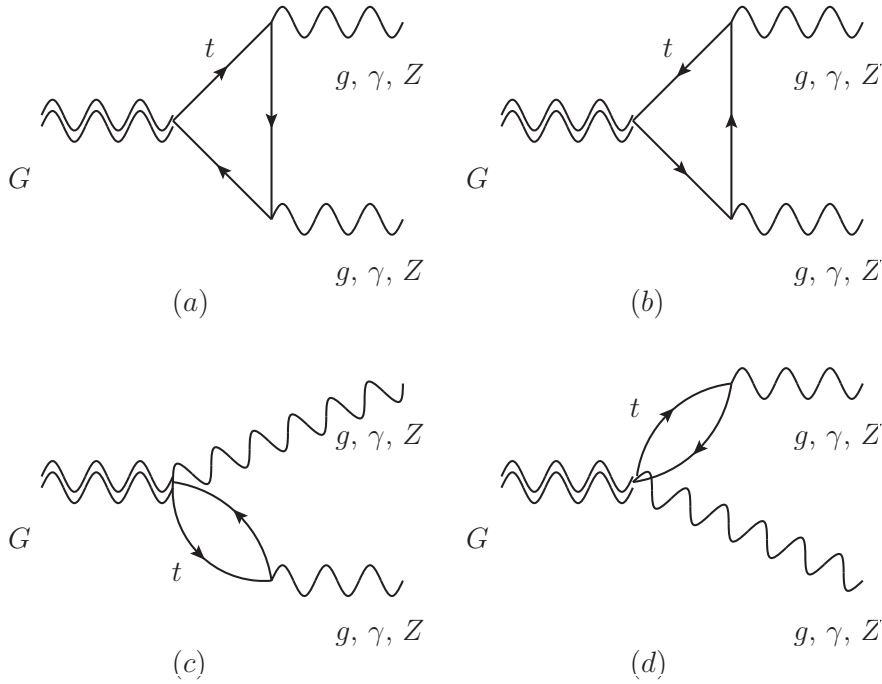


Figure 1: Feynman diagrams for the one-loop top-quark contributions to the Ggg , $G\gamma\gamma$, $G\gamma Z$, and GZZ vertices.

graviton G with the emphasis on the unconventional power counting rules and the possible significance of the top-quark loop contributions to the productions and decays of G . The present model provides the minimal setup to realize this scenario.

3 Top-loop Effects to Effective Couplings of G

Before proceeding to discuss the LHC phenomenology of the KK graviton G , let us begin by discussing what the implication is for the power counting rules in Eq. (3). By assumption, the right-handed top quark coupling c_{tt} is of $\mathcal{O}(1)$, while the couplings with g , γ and Z are suppressed by the extra-dimensional volume dilution with the order of $\alpha_{(s)}/(4\pi)$. Thus, it is expected that the top-quark one-loop contributions to the couplings between the KK graviton G and these SM gauge bosons as shown in Fig. 1 should be at the same order as the tree-level ones. In other words, the leading-order (LO) interactions of G with g , γ and Z should be the combination of these two contributions. Therefore, it is useful to define the

following LO effective couplings, given by

$$\begin{aligned}
c_{gg}^{\text{eff}} &= \begin{cases} c_{gg}(m_G) + c_{tt}A_G\left(\frac{4m_t^2}{m_G^2}\right), & m_G \geq m_t \\ c_{gg}(m_t) + c_{tt}B_G\left(\frac{4m_t^2}{m_G^2}\right), & m_G < m_t \end{cases} \\
c_{\gamma\gamma}^{\text{eff}} &= \begin{cases} c_{\gamma\gamma}(m_G) + 2Q_t^2N_c c_{tt}A_G\left(\frac{4m_t^2}{m_G^2}\right), & m_G \geq m_t \\ c_{\gamma\gamma}(m_t) + 2Q_t^2N_c c_{tt}B_G\left(\frac{4m_t^2}{m_G^2}\right), & m_G < m_t \end{cases} \quad (6)
\end{aligned}$$

where $Q_t = 2/3$, $N_c = 3$ and $m_t = 173.1$ GeV represent the top quark electric charge, color and mass, respectively. We have also defined the following functions

$$\begin{aligned}
A_G(\tau) &\equiv -\frac{1}{36} [9\tau(\tau+2)f(\tau) + 6(5\tau+4)g(\tau) - 39\tau - 35 + 12\ln(\tau/4)], & \tau \leq 4 \\
B_G(\tau) &\equiv -\frac{1}{36} [9\tau(\tau+2)f(\tau) + 6(5\tau+4)g(\tau) - 39\tau - 35], & \tau > 4 \quad (7)
\end{aligned}$$

with

$$f(\tau) = \begin{cases} -[\operatorname{arctanh}(\sqrt{1-\tau}) - i\pi/2]^2, & \tau < 1 \\ \arcsin^2(1/\sqrt{\tau}), & \tau \geq 1 \end{cases} \quad (8)$$

$$g(\tau) = \begin{cases} \sqrt{1-\tau}[\operatorname{arctanh}(\sqrt{1-\tau}) - i\pi/2], & \tau < 1 \\ \sqrt{\tau-1} \arcsin(1/\sqrt{\tau}), & \tau \geq 1 \end{cases} \quad (9)$$

Note that in order to keep the gauge invariance of the right-handed-top-quark- G coupling, we have included the coupling of $\bar{t}_R G^{a(\mu\gamma\nu)} t_R G_{\mu\nu}$ in the Lagrangian of Eq. (2) by the covariant derivative of t_R . As a result, we need to incorporate the one-loop Feynman diagrams (c) and (d) of Fig. 1 besides the triangle ones calculated in Ref. [14]. However, as shown in Appendix A, their contributions vanish identically when we apply the KK graviton and EW boson on-shell conditions.

Compared the top-loop contributions to the Ggg and $G\gamma\gamma$ couplings in Ref. [14], we have extended the valid range of the expressions to the whole parameter space, no matter whether m_G is larger than $2m_t$ or not. In addition, the top-quark one-loop diagrams in Fig. 1 are UV divergent, so that we need to perform the renormalization skill to remove the corresponding UV divergence, which results in the renormalization scale dependence when defining the tree-level couplings $c_{gg(\gamma\gamma)}$ and the modification of the loop functions from A_G to B_G when m_G decreases below m_t . Concretely, when $m_G > m_t$, the appropriate renormalization scale should be m_G since the KK graviton is on-shell at this scale. In comparison, if $m_G < m_t$, we need to integrate out the top quark fields first in the theory so that the renormalization scale should be chosen to be m_t . Nevertheless, the final effective coupling $c_{gg(\gamma\gamma)}^{\text{eff}}$ is a continuous function of $4m_t^2/m_G^2$, whereas its first

derivative is not, which is the reflection of the renormalization effects. A further justification of the expression in Eq. (6) is provided by looking at the so-called decoupling limit in which $m_t/m_G \rightarrow \infty$. It is easy to check that in this limit the loop function $B_G(4m_t^2/m_G^2)$ vanishes, which agrees with the decoupling theorem. In Fig. 2, we show the typical behavior of the effective couplings for $G\gamma\gamma$ and Ggg as functions of the KK graviton mass m_G , which clearly displays the decoupling tendency of top-loop effect when G becomes lighter.

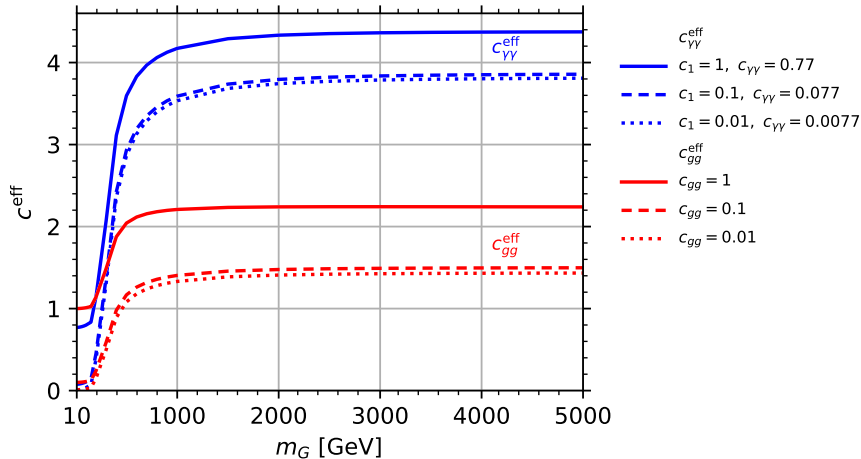


Figure 2: Effective KK graviton couplings as functions of the KK graviton mass, where $c_{tt} = 1$ is chosen and the solid, dashed and dotted lines correspond to c_1 and $c_{gg} = 1, 0.1$ and 0.01 , while the blue and red lines are for the effective coupling between the KK graviton and photons and gluons, respectively.

4 Production Cross Section of the KK Graviton

In our model, the inclusive KK graviton production of $pp \rightarrow G$ at the LHC is given by a tree level contribution to $gg \rightarrow G$ as well as those via right-handed top loops denoted as “LO” (at the same order). For the estimation of “NLO” contributions, both 1 and 2-loop level calculations are required because the right-handed top loops already exist at “LO”. For a rough estimation with the NLO QCD accuracy, we depict $pp \rightarrow G$ for the pp collisions at 13 TeV as the function of the KK graviton mass in the range of 2–5 TeV in Fig. 3, where we have assumed that gluons can only interact with the KK graviton. In our numerical analysis, we use MADGRAPH5_AMC@NLO [18, 19, 20, 21] with the LO/NLO NNPDF2.3 [22]. We also take $\alpha_s c_{gg}/(4\pi\Lambda) = (3 \text{ TeV})^{-1}$, which does not affect the K factors.

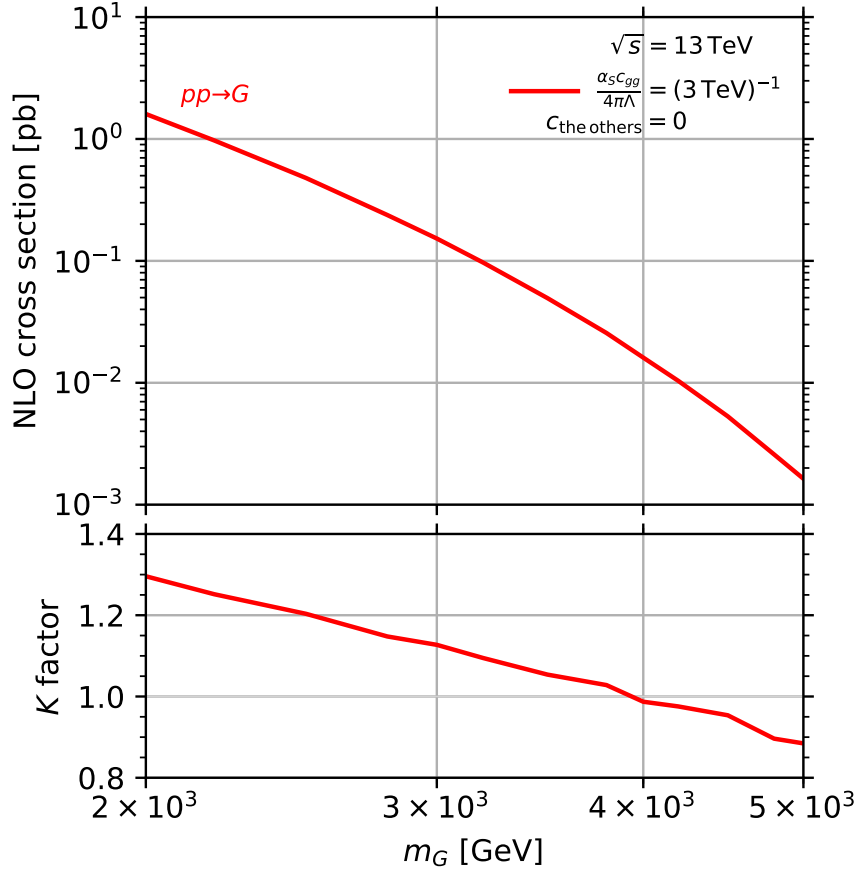


Figure 3: Production cross sections of the KK graviton with the NLO accuracy at the 13 TeV LHC (upper panel) and K factors (lower panel) as functions of the KK graviton mass, where $\alpha_s c_{gg}/(4\pi\Lambda) = (3 \text{ TeV})^{-1}$ and the KK graviton couplings to the others including the top quark are zero.

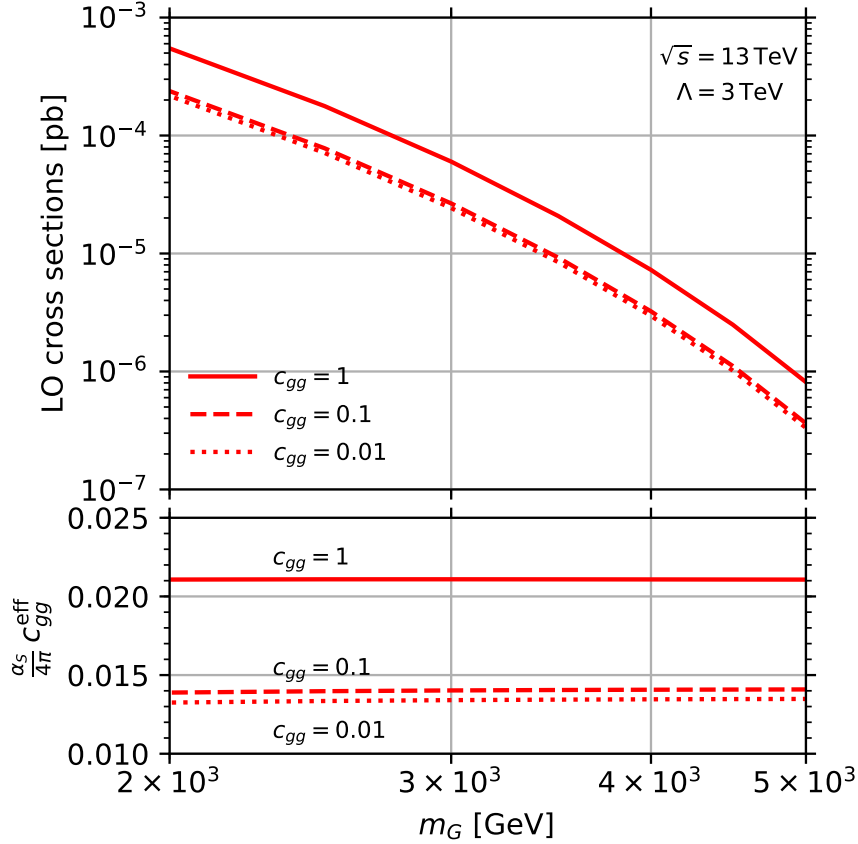


Figure 4: Production cross sections of the KK graviton with the “LO” accuracy (upper panel), which includes the production via the right-handed top loop at the 13 TeV LHC, and $\alpha_s c_{gg}^{\text{eff}}/(4\pi\Lambda)$ (lower panel) as functions of the KK graviton mass, where $\Lambda = 3 \text{ TeV}$ and $c_{tt} = 1$, along with three choices of $c_{gg} = 1$ (solid), 0.1 (dashed) and 0.01 (dotted).

Note that the values of K are smaller than 1 at the high mass region when the KK graviton only couples to a gluon current. For the KK graviton mass range considered, the K factors are within 30 % discrepancy from 1, corresponding to a tree-level production. Since these factors become larger as the KK graviton mass decreases, in this study we only concentrate on the high mass range of $m_G = 2\text{--}5 \text{ TeV}$.

As these NLO cross sections are rough estimations, we use the “LO” cross section, which includes the production via the right-handed top loops in our calculation. For simplicity, we take $c_{tt} = 1$ in the whole analysis. The results of the “LO” cross section as a function of KK graviton mass are shown in Fig. 4. The effective coupling between the KK graviton and a gluon current, $(4\pi)^{-1}\alpha_s c_{gg}^{\text{eff}}$, is shown in the lower panel. Because of the high KK graviton mass, the top-loop

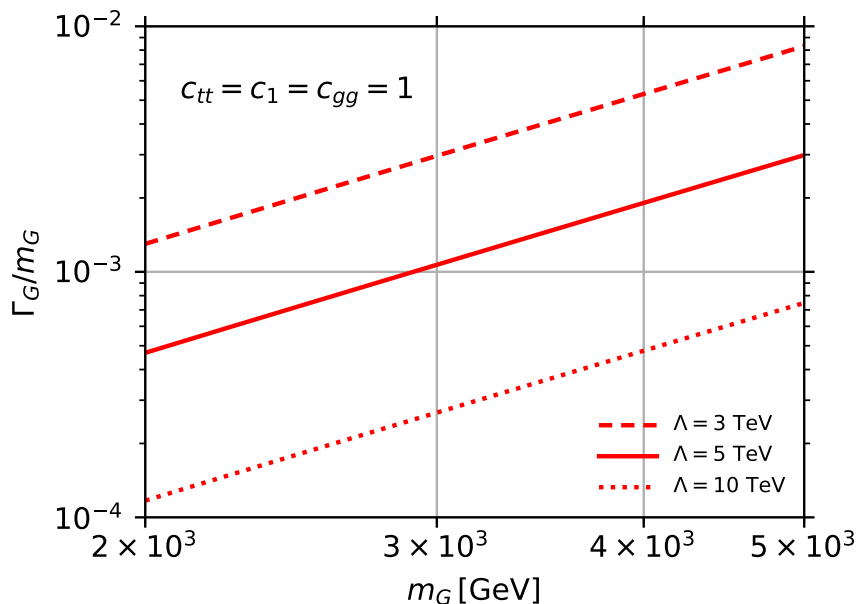


Figure 5: Total width of the KK graviton to its mass as a function of the KK graviton mass, where $c_{tt} = c_1 = c_{gg} = 1$ with $\Lambda = 3$ (dashed), 5 (solid) and 10 (dotted) TeV.

effect is almost the same as that in Fig. 2 with $m_G = 2\text{--}5$ TeV. In addition, the lines for $\alpha_s c_{gg}^{\text{eff}}/(4\pi\Lambda)$ at $c_{gg} = 0.1$ and $c_{gg} = 0.01$ are in the same order because of the large contribution from the top-loop. In the following sections, we will use $c_{gg} = 1$ in our analysis as it is a natural value from a profile view of the gluon field in a bulk. The top-loop contributions are the same order as those in the tree-level as shown in Fig. 2.

5 Decays of the KK Graviton

Our signals are $t\bar{t}$, gg , $\gamma\gamma$, γZ and ZZ through the decays of the KK graviton resonance. We assume that the narrow width approximation can be applied for the relativistic Breit-Wigner resonance of the KK graviton. In this case, the cross sections of the signals are obtained by

$$\sigma(pp \rightarrow G \rightarrow XX') = \sigma(pp \rightarrow G)B(G \rightarrow XX'), \quad (10)$$

where $\sigma(pp \rightarrow G)$ is the production cross section of the KK graviton and $B(G \rightarrow XX')$ correspond to the branching ratios of the KK graviton decaying into the particle pairs of XX' with $XX' = t\bar{t}$, gg , $\gamma\gamma$, γZ , and ZZ . Figure 5 shows the KK graviton (G) total width divided by its mass, Γ_G/m_G . Note that MADWIDTH [23]

Table 1: Branching ratios of the KK graviton for $c_{tt} = c_1 = c_{gg} = 1$.

m_G [GeV]	Branching ratios [%]				
	$t\bar{t}$	gg	$\gamma\gamma$	γZ	ZZ
2000					
–	~ 100	0.5	0.001	6×10^{-4}	1×10^{-4}
5000					

provides the partial decay rates numerically for each mass point. The resonance is very narrow as $\Gamma_G/m_G < 1\%$ in a range of 2–5 TeV of m_G with bench mark points of $\Lambda = 3, 5, 10$ TeV. respectively.

The partial widths for $G \rightarrow XX'$ are given by

$$\Gamma(G \rightarrow t\bar{t}) = \frac{N_c}{320\pi} \frac{c_{tt}^2 m_G^3}{\Lambda^2} \left(1 - \frac{4m_t^2}{m_G^2}\right)^{3/2} \left(1 + \frac{8}{3} \frac{m_t^2}{m_G^2}\right), \quad (11)$$

$$\Gamma(G \rightarrow \gamma\gamma) = \frac{m_G^3}{80\pi\Lambda^2} \left| \frac{\alpha}{4\pi} c_{\gamma\gamma}^{\text{eff}} \right|^2, \quad (12)$$

$$\Gamma(G \rightarrow gg) = \frac{m_G^3}{10\pi\Lambda^2} \left| \frac{\alpha_s}{4\pi} c_{gg}^{\text{eff}} \right|^2, \quad (13)$$

$$\begin{aligned} \Gamma(G \rightarrow \gamma Z) &= \frac{m_G^3}{160\pi\Lambda^2} \left(\frac{\sin 2\theta_W}{\cos^2 \theta_W} \right)^2 \left(1 - \frac{m_Z^2}{m_G^2}\right)^3 \\ &\times \left(1 + \frac{m_Z^2}{2m_G^2} + \frac{m_Z^4}{6m_G^4}\right) \left| \frac{\alpha c_{\gamma\gamma}^{\text{eff}}}{4\pi} \right|^2, \end{aligned} \quad (14)$$

$$\begin{aligned} \Gamma(G \rightarrow ZZ) &= \frac{m_G^3}{80\pi\Lambda^2} \tan^4 \theta_W \left(1 - \frac{4m_Z^2}{m_G^2}\right)^{1/2} \\ &\times \left(1 - \frac{3m_Z^2}{m_G^2} + \frac{6m_Z^4}{m_G^4}\right) \left| \frac{\alpha c_{\gamma\gamma}^{\text{eff}}}{4\pi} \right|^2. \end{aligned} \quad (15)$$

Note that $\Gamma(G \rightarrow t\bar{t})$ contains an extra factor of 1/2 compared to that when the KK graviton G couples to both the left- and right-handed top quarks. The decay mode with γZ in our model appears due to the non-universal couplings of G to the weak gauge bosons. Since in the following we only consider the heavy KK graviton case in which $m_G \gg m_Z$, we can take the zero Z mass limit when computing the one-loop corrected effective couplings, which are reduced to $c_{\gamma\gamma}^{\text{eff}}$ as in Eqs. (15) and (16).

As shown in Table 1, the $t\bar{t}$ channel has almost 100 % branching ratio for the KK graviton mass in 2–5 TeV. The other channels have small fractions of the branching ratios, which can still lead to some constraints on our model parameters as a diphoton final state is a clean experimental signature. The branching ratios

Table 2: Constraints from resonance searches based on $\sqrt{s} = 13$ TeV at the LHC with the observed 95% CL upper limits on the resonant production cross section (σ) \times branching ratio (B) (\times acceptance (A)).

Decay mode	Reference	Limit Table/Figure	Limit on	L (fb $^{-1}$)
$t\bar{t}$	CMS-PAS-B2G-17-017 [24]	Table 2	$\sigma(\text{narrow - width } Z') \times B$	36
gg	CMS arXiv:1806.00843 [25]	Table 2 (gg)	$\sigma(\text{narrow - width Res.}) \times B \times A$	27+36
$\gamma\gamma$	CMS-PAS-EXO-17-017 [26]	Fig. 3 (middle)	$\sigma(G_{\text{RS}}) \times B$	35.9
γZ	CMS-PAS-EXO-17-005 [27]	Fig. 6a	$\sigma(\text{narrow - width Res.}) \times B$	35.9
ZZ	ATLAS-CONF-2018-016 [28]	Fig. 14b	$\sigma(G_{\text{RS}}) \times B$	79.8

of gg , $\gamma\gamma$, γZ and ZZ channels are 0.5 %, 0.001 %, 6×10^{-4} %, and 1×10^{-4} %, respectively. As we concentrate on a high mass region of the KK graviton, all decay modes in our model are kinematically allowed and the corresponding branching ratios are almost fixed in the whole mass range.

6 Constraints from the 13 TeV LHC data

Our target signals come from the decay of the KK graviton resonance in the s -channel. The $\sqrt{s} = 13$ TeV LHC results are taken to limit the model in the high mass region of the KK graviton. We take $c_{tt} = c_1 = c_{gg} = 1$ in Eq. (2) in our analysis. We choose the CMS data for $t\bar{t}$, gg (dijet), $\gamma\gamma$, γZ [24, 25, 26, 27] and ATLAS data for ZZ [28] final states. In Table 2, we list the current results for the resonance searches, which are used to constrain the model parameter space of the top-philic bulk RS model. In particular, the constraint on a $t\bar{t}$ resonance is given in terms of the narrow-width Z' search in Ref. [24], while the bounds on the model independent narrow-width resonances are studied for gg (dijet) and γZ channels in Ref. [25, 27]. In addition, we use the gluon-gluon (gg) resonance result for our dijet analysis as the dominant contribution stems from the gluon fusion. In Refs. [26, 28], the RS graviton is considered for $\gamma\gamma$ and ZZ modes. For the gg (dijet) mode, a limit can be given for the fiducial cross section of $\sigma(pp \rightarrow G) \times B \times A$, where A is acceptance. We apply the fiducial cuts at the parton level to obtain the fiducial cross section. The other limits for $\sigma(pp \rightarrow G) \times B$ are also available as shown in the column of “Limit on” in Table 2. The production cross sections of the KK graviton and its decay branching ratios have been discussed in Secs. 4 and 5, respectively. We note that we extract the data from the figures by using WEBPLOTDIGITIZER [29] for $\gamma\gamma$, γZ , and ZZ modes.

Figure. 6 shows the constraints on the inverted coupling Λ from the observed 95 % CL lower limits of the resonance searches listed in Table 2. The $t\bar{t}$ final state

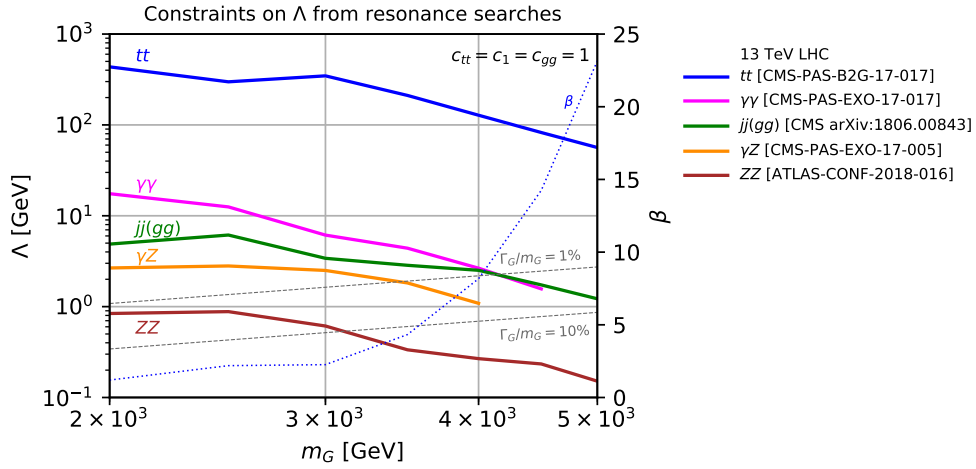


Figure 6: Constraints on Λ as a function of the KK graviton mass from the observed 95% CL lower limits of the resonance searches at the 13 TeV LHC with the regions below each line excluded, where the grey dashed and blue dotted lines correspond to the KK graviton width-to-mass ratio and $\beta = k/\bar{M}_{\text{Pl}}$, respectively.

of the KK graviton resonance signal gives the strongest limit as expected from its almost 100 % branching ratio. Although the branching fraction of 0.001 % for the $\gamma\gamma$ channel is small, it leads to the next strongest limit due to its clean signature in the experiment. The dijet signal (gg resonance), which provides the second largest branching ratio of G decays, yields the comparable result for $m_G \sim 4$ –4.5 TeV but a weaker limit for $m_G < 4$ TeV than $\gamma\gamma$ because the acceptance after cuts is small. For the KK graviton production and its decay mode of gg at the parton level, the efficiency is about 0.3 for the 2–5 TeV mass after imposing $|\eta_j| < 2.5$ and $|\Delta\eta_j| < 1.3$, where η_j is the pseudorapidity of each jet. It is clear that the cut of $|\Delta\eta_j| < 1.3$ abandons many signal events. For example, for $m_G = 2$ TeV, 67% signal events are excluded with $|\Delta\eta_j| < 1.3$ after imposing $|\eta_j| < 2.5$ beforehand. Because the jj background is from t and u channels besides the s one, forward and backward regions should be cut to reduce the background events. Our signal is a resonance (s -channel), the central region has relatively more events than the background ones. Note that the structure of matrix elements is important. On the other hand, the angular momentum (i.e., s or d -wave) is essential for the angular distribution, which can be used to distinguish spins of the signal resonances. We now concentrate on the total cross sections. As seen in Fig. 6, the strong signals are given by the $t\bar{t}$, $jj(gg)$, γZ , and ZZ modes. In the figure, we show $\Gamma_G/m_G = 1\%$ and 10% points with grey dashed lines as we assume a narrow-width in our calculations of the signals and use the information of the narrow-width resonances from the experimental data. Lower limits on Λ for each mass point in our model are less than 500 GeV, which are different from those of several TeV or several 10 TeV on Λ in the universal case with m_G in the range of 2–5 TeV [4]. In order to relate our phenomenological parameters m_G and Λ to the bulk geometry more transparently, we have defined a new variable $\beta \equiv (3.83)^{-1} \times m_G/\Lambda = k/\bar{M}_{\text{Pl}}$ and shown its upper limits as the dashed curve at each G mass in Fig.6. As a result, the values of $\beta \geq 0.01$ on the curve imply large 5D curvatures k , which cannot be obtained by a simple assumption in the string theory [30]. Concretely, the corresponding radii of the extra dimension should vary from $9.6/\bar{M}_{\text{Pl}}$ at $m_G = 2$ TeV to $0.53/\bar{M}_{\text{Pl}}$ when $m_G = 5$ TeV.

We now examine the largest allowed cutoff scale Λ_{cut} in our model, which can be derived from the violation of the perturbative unitarity. It is well-known that Λ_{cut} becomes lower for the non-universal coupling case [31, 32]. In the present model, the strongest constraints can be obtained from the s -wave processes of $t_R\bar{t}_R \rightarrow gG$

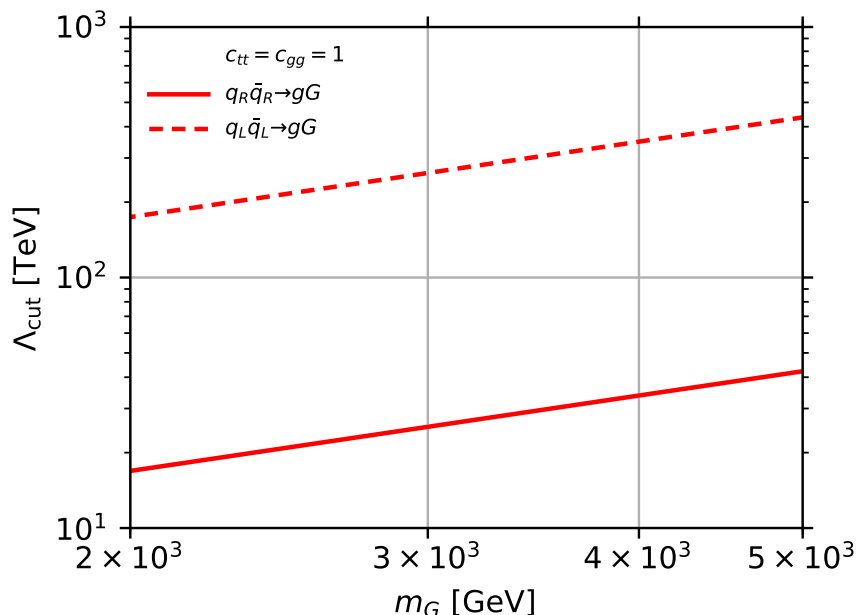


Figure 7: The cutoff scale Λ_{cut} as a function of the KK graviton mass with the region below each line allowed.

and $q_L \bar{q}_L \rightarrow gG$, in which the 0-helicity KK graviton production can generate the amplitudes proportional to $[(c_g - c_{tR}) \text{ or } (c_g - c_{qL})] \times s^{3/2}/(m_G^2 \Lambda)$ [32], where the subscripts R and L denote the projection operators of $(1 \pm \gamma_5)/2$, respectively. We utilize the formula in Ref. [32] and depict Λ_{cut} in Fig. 7, where the perturbative unitarity is lost when $\text{Re}(\text{amplitude}) > 1/2$. Figure 7 shows that the $t_R \bar{t}_R \rightarrow gG$ process gives a stronger limit on the cutoff of Λ_{cut} for each mass point than the $q_L \bar{q}_L \rightarrow gG$ one. The values of Λ_{cut} can be of several 10 TeV, which are much higher than the experimental lower limit of $\Lambda < 500$ GeV given in Fig. 6.

7 Summary

We have concentrated on the bulk RS model, in which the KK graviton G interacts strongly with the right-handed top quark due to the profile of the right-handed top quark localized near the IR brane. In our model, as the color $SU(3)_c$ and hypercharge $U(1)_Y$ gauge fields propagate in the bulk, the corresponding couplings with the KK gravitons are suppressed by a volume factor. In contrast, the other SM particle fields are localized near the UV brane, which give exponentially small couplings of these particles to G . We have studied the constraints on the model parameter space based on the current 13 TeV LHC results for the first/lightest KK

graviton. Our LHC signals are $t\bar{t}$, $\gamma\gamma$, $jj(gg)$, γZ , and ZZ via the decays of the KK graviton resonance. In our estimations, we have included the top-loops for the production of the KK graviton and its decays. We have found that the strongest limit is from the $t\bar{t}$ mode, which gives $\mathcal{O}(100)$ GeV for the lower bounds of Λ for $m_G = 2\text{--}5$ TeV, which are smaller than those in the universal coupling case. Our rough unitarity bounds in the model suggest that Λ should be smaller than several 10 TeV for $m_G = 2\text{--}5$ TeV. A parameter region in our non-universal model survived roughly between $\mathcal{O}(100)$ GeV $< \Lambda <$ several 10 TeV for $m_G = 2\text{--}5$ TeV.

Finally, we would like to remark that one interesting prediction of our present scenario is the presence of light KK states of bulk gauge bosons, such as massive KK gluons. When the bulk geometry is a slice of AdS₅ spacetime with its curvature (length) represented as k (L), the mass of the first massive KK gluon g^1 is found to be $m_{g^1} \approx 2.4ke^{-kL}$, and its coupling to the right-handed top quark is $g_{g^1} \sim g_s(kL)^{1/2}$. When $kL \sim 30$, it is predicted that this mass of this KK gluon is of $\mathcal{O}(\text{TeV})$, and more strongly coupled to quarks than the usual gluon, which is promising to be probed at colliders. In fact, this massive KK gluon g^1 is even parametrically lighter than the first KK state of graviton whose mass is $m_G \approx 3.8ke^{-kL}$. Thus, g^1 is expected to be more easily discovered than G , which violates our implicit assumptions that the KK graviton G is the first KK state to be seen at the LHC. One way to avoid this problem is to find a way to make the KK graviton G lighter than the KK gluon g^1 . It is shown in Ref. [32] that we can achieve this by adding the boundary kinetic terms for the bulk graviton at both UV and IR branes.

It is interesting to compare the phenomenology of this top-philic KK gluon [33] with that of the top-philic KK graviton. In the light of the Landau-Yang theorem, the massive KK graviton cannot be singly produced on-shell via the gluon fusion, neither can it decay to the diphoton or digluon final states. Unlike the colorless top-philic vector boson studied in Ref. [34], the KK gluon here carries color quantum numbers. Thus, it is shown in Ref. [33] that, due to its nonvanishing constant 5D field profile in the IR, g^1 can still have sizable couplings to the light quarks, leading to that g^1 is mostly produced on-shell by the $q\bar{q} \rightarrow g^1$ with q denoting light quarks contained in the proton. On the other hand, we expect that the gluon fusion can also give rise to the substantial g^1 production at the LHC, with the channels as $gg \rightarrow g^1g$ in which g^1 decays to a $t\bar{t}$ pair, or $gg \rightarrow g^1 \rightarrow t\bar{t}$, where g^1 is created off-shell [34]. However, in contrast to the case in Ref. [34],

we can prove by some simple estimations that both processes are dominated by tree-level diagrams. Take, for instance, the g^1 on-shell production associated with a jet from the gluon fusion. At the tree level, the amplitude should be of order $\sim g_s^2$. In comparison, the one-loop Feynman diagrams predict the amplitude to be $\sim g_s^4(kL)^{1/2}/(16\pi^2) \sim g_s^2(kL)^{-1/2}$, where we have used our previous power counting rule $\alpha_s/(4\pi) \sim 1/(kL)$ in the discussion of the massive KK graviton. Obviously, the one-loop amplitude is suppressed by the additional factor of $(kL)^{-1/2}$ compared with the tree-level one. This result is starkly contrasted with that of the massive KK graviton G considered in the present paper.

A Additional Diagrams

Due to the gauge covariance of the right-handed top quark kinetic terms, we should have two extra diagrams (c) and (d) in Fig. 1 besides of the triangle diagrams considered previously in Ref. [14]. In this subsection, we calculate their contributions to the effective Ggg couplings according to the interacting Lagrangian in Eqs. (2) and (4). The calculations of the $G\gamma\gamma$, $G\gamma Z$ and GZZ couplings follow the same procedure.

Note that only the massive graviton couples to the right-handed top quark field strongly, so that the amplitude of the Feynman diagram (c) is

$$\begin{aligned}
i\mathcal{M}_{(c)} &= \frac{g^2 c_{tt}}{2\Lambda} \text{tr}(T^a T^b) (C_{\mu\nu,\sigma\kappa} - \eta_{\mu\nu}\eta_{\sigma\kappa}) \\
&\times \frac{1}{(2\pi)^4} \int d^4l \left(\frac{\text{Tr}[\gamma^\kappa P_R(\not{l} + m_t)\gamma_\rho(\not{l} + \not{k}_1 + m_t)]}{(l^2 - m_t^2)[(l + k_1)^2 - m_t^2]} \right) \\
&\times \epsilon^{\delta\mu\nu}(P)\epsilon^{\rho*}(k_1)\epsilon^{\sigma*}(k_2) \\
&= \epsilon^{\delta\mu\nu}(P)\epsilon^{\rho*}(k_1)\epsilon^{\sigma*}(k_2) \frac{ig^2 c_{tt} \delta^{ab}}{4\Lambda} (C_{\mu\nu,\sigma\kappa} - \eta_{\mu\nu}\eta_{\sigma\kappa}) \frac{1}{16\pi^2} \int_0^1 dx \\
&\left\{ [4x(1-x)(\eta_\rho^\kappa k_1^2 - k_1^\kappa k_{1\rho})] \left(\frac{2}{\epsilon} - \gamma_\omega + \ln \frac{4\pi\mu^2}{m_t^2 - x(1-x)k_1^2} \right) \right\}, \quad (16)
\end{aligned}$$

where $\text{tr}(T^a T^b) = \delta^{ab}/2$, the tensor $C_{\mu\nu,\sigma\kappa}$ is defined as in the appendix of Ref. [35], and k_1 denotes the momentum of one external gluon. Consequently, if we use the on-shell conditions $k_1^2 = 0$ and $k_1^\rho \epsilon_\rho^*(k_1) = 0$, the above amplitude vanishes. The same argument applies to the amplitude (d) in Fig. 1, except for the exchange $k_1 \rightarrow k_2$. Note that the amplitude obtained in Eq. (16) satisfies the Ward Identities for the external gluon k_1 , so that this result is quite general in the view of the gauge invariance of QCD. Therefore, these diagrams do not contribute.

Acknowledgements We thank Professor Kentarou Mawatari and Dr. Chen Zhang for their valuable comments. This work was supported in part by National Center for Theoretical Sciences, MoST (MoST-104-2112-M-007-003-MY3 and MoST-107-2119-M-007-013-MY3), NSFC (11547008) and the National Science Centre (Poland) research project (DEC-2014/15/B/ST2/00108).

References

- [1] L. Randall and R. Sundrum, *Phys. Rev. Lett.* **83**, 3370 (1999) doi:10.1103/PhysRevLett.83.3370 [hep-ph/9905221].
- [2] H. M. Lee, M. Park and V. Sanz, *Eur. Phys. J. C* **74**, 2715 (2014) doi:10.1140/epjc/s10052-014-2715-8 [arXiv:1306.4107 [hep-ph]].
- [3] H. M. Lee, M. Park and V. Sanz, *JHEP* **1405**, 063 (2014) doi:10.1007/JHEP05(2014)063 [arXiv:1401.5301 [hep-ph]].
- [4] S. Kraml, U. Laa, K. Mawatari and K. Yamashita, *Eur. Phys. J. C* **77**, no. 5, 326 (2017) doi:10.1140/epjc/s10052-017-4871-0 [arXiv:1701.07008 [hep-ph]].
- [5] T. D. Rueter, T. G. Rizzo and J. L. Hewett, *JHEP* **1710**, 094 (2017) doi:10.1007/JHEP10(2017)094 [arXiv:1706.07540 [hep-ph]].
- [6] W. D. Goldberger and M. B. Wise, *Phys. Rev. D* **60**, 107505 (1999) doi:10.1103/PhysRevD.60.107505 [hep-ph/9907218].
- [7] H. Davoudiasl, J. L. Hewett and T. G. Rizzo, *Phys. Lett. B* **473**, 43 (2000) doi:10.1016/S0370-2693(99)01430-6 [hep-ph/9911262].
- [8] A. Pomarol, *Phys. Lett. B* **486**, 153 (2000) doi:10.1016/S0370-2693(00)00737-1 [hep-ph/9911294].
- [9] S. Chang, J. Hisano, H. Nakano, N. Okada and M. Yamaguchi, *Phys. Rev. D* **62**, 084025 (2000) doi:10.1103/PhysRevD.62.084025 [hep-ph/9912498].
- [10] H. Davoudiasl, J. L. Hewett and T. G. Rizzo, *Phys. Rev. D* **63**, 075004 (2001) doi:10.1103/PhysRevD.63.075004 [hep-ph/0006041].
- [11] B. M. Dillon and V. Sanz, *Phys. Rev. D* **96**, no. 3, 035008 (2017) doi:10.1103/PhysRevD.96.035008 [arXiv:1603.09550 [hep-ph]].

- [12] B. M. Dillon, C. Han, H. M. Lee and M. Park, *Int. J. Mod. Phys. A* **32**, no. 33, 1745006 (2017) doi:10.1142/S0217751X17450063 [arXiv:1606.07171 [hep-ph]].
- [13] B. M. Dillon, B. K. El-Menoufi, S. J. Huber and J. P. Manuel, arXiv:1708.02953 [hep-th].
- [14] C. Q. Geng and D. Huang, *Phys. Rev. D* **93**, no. 11, 115032 (2016) doi:10.1103/PhysRevD.93.115032 [arXiv:1601.07385 [hep-ph]].
- [15] H. M. Lee, D. Kim, K. Kong and S. C. Park, *JHEP* **1511**, 150 (2015) doi:10.1007/JHEP11(2015)150 [arXiv:1507.06312 [hep-ph]].
- [16] E. Ponton, doi:10.1142/9789814390163_0007 arXiv:1207.3827 [hep-ph].
- [17] C. Csaki, J. Heinonen, J. Hubisz, S. C. Park and J. Shu, *JHEP* **1101**, 089 (2011) doi:10.1007/JHEP01(2011)089 [arXiv:1007.0025 [hep-ph]].
- [18] J. Alwall *et al.*, *JHEP* **1407**, 079 (2014) doi:10.1007/JHEP07(2014)079 [arXiv:1405.0301 [hep-ph]].
- [19] P. Mastrolia, E. Mirabella and T. Peraro, *JHEP* **1206**, 095 (2012) Erratum: [*JHEP* **1211**, 128 (2012)] doi:10.1007/JHEP11(2012)128, 10.1007/JHEP06(2012)095 [arXiv:1203.0291 [hep-ph]].
- [20] T. Peraro, *Comput. Phys. Commun.* **185**, 2771 (2014) doi:10.1016/j.cpc.2014.06.017 [arXiv:1403.1229 [hep-ph]].
- [21] V. Hirschi and T. Peraro, *JHEP* **1606**, 060 (2016) doi:10.1007/JHEP06(2016)060 [arXiv:1604.01363 [hep-ph]].
- [22] R. D. Ball *et al.*, *Nucl. Phys. B* **867**, 244 (2013) doi:10.1016/j.nuclphysb.2012.10.003 [arXiv:1207.1303 [hep-ph]].
- [23] J. Alwall, C. Duhr, B. Fuks, O. Mattelaer, D. G. Öztürk and C. H. Shen, *Comput. Phys. Commun.* **197**, 312 (2015) doi:10.1016/j.cpc.2015.08.031 [arXiv:1402.1178 [hep-ph]].
- [24] CMS Collaboration [CMS Collaboration], CMS-PAS-B2G-17-017.
- [25] A. M. Sirunyan *et al.* [CMS Collaboration], doi:10.3204/PUBDB-2018-02190 arXiv:1806.00843 [hep-ex].

- [26] CMS Collaboration [CMS Collaboration], CMS-PAS-EXO-17-017.
- [27] CMS Collaboration [CMS Collaboration], CMS-PAS-EXO-17-005.
- [28] The ATLAS collaboration [ATLAS Collaboration], ATLAS-CONF-2018-016.
- [29] <https://automeris.io/WebPlotDigitizer/> Accessed June 28 2018
- [30] H. Davoudiasl, J. L. Hewett and T. G. Rizzo, Phys. Rev. Lett. **84**, 2080 (2000) doi:10.1103/PhysRevLett.84.2080 [hep-ph/9909255].
- [31] P. Artoisenet *et al.*, JHEP **1311**, 043 (2013) doi:10.1007/JHEP11(2013)043 [arXiv:1306.6464 [hep-ph]].
- [32] A. Falkowski and J. F. Kamenik, Phys. Rev. D **94**, no. 1, 015008 (2016) doi:10.1103/PhysRevD.94.015008 [arXiv:1603.06980 [hep-ph]].
- [33] B. Lillie, L. Randall and L. T. Wang, JHEP **0709**, 074 (2007) doi:10.1088/1126-6708/2007/09/074 [hep-ph/0701166].
- [34] N. Greiner, K. Kong, J. C. Park, S. C. Park and J. C. Winter, JHEP **1504**, 029 (2015) doi:10.1007/JHEP04(2015)029 [arXiv:1410.6099 [hep-ph]].
- [35] T. Han, J. D. Lykken and R. J. Zhang, Phys. Rev. D **59**, 105006 (1999) doi:10.1103/PhysRevD.59.105006 [hep-ph/9811350].